# NUMERICAL ANALYS OF THE DYNAMIC OF A GAS BUBBLE IN A CENTRIFUGAL PUMP IMPELLER

**Felipe C. Ancajima, felancajima@gmail.com**
**Henrique Stel, stel.henrique@gmail.com**
**Moisés M. A. Neto, mneto@utfpr.edu.br**
**Dalton Bertoldi, daltonbertoldi@utfpr.edu.br**
**Rigoberto E. M. Morales, rmorales@utfpr.edu.br**
NUEM/PPGEM/UTFPR, Av. Sete de Setembro 3165, CEP. 80230-901, Curitiba-PR-Brasil

***Abstract.*** *Centrifugal pumps are widely used in the oil industry as an artificial lift technique. The existing gas in some oil reservoirs can cause head degradation in such pumps. The performance deterioration implies a reduced ability to raise pressure, which reduces the well oil production rate thus resulting in economic losses. However, the behavior of gas-liquid mixtures in centrifugal pumps is a complex subject that is virtually unexplored in the literature, and the numerical methods addressing this issue are scant to say the least. This work proposes a numerical study on the dynamics of a gas bubble inside the first stage of a radial centrifugal pump impeller. To achieve this objective, a particle-tracking approach is employed through a commercial CFD software. The study aims at analyzing the relevance of the drag force, the force due to the pressure gradient and the virtual mass force acting on a bubble flowing through the liquid in the rotating impeller channel. Numerical results are compared with previous experimental data obtained for two-phase flow of water and air through the same pump model. The behavior of the bubbles inside the impeller, the role played by each force in their motion and the functional relations between those forces and the operating conditions of the pump are all topics of concern to the present investigation.*

***Keywords****: ESP, two-phase flow, interfacial forces, CFD.*

## 1. INTRODUCTION

Artificial lift methods are used by the petroleum industry to increase the production rate in situations where naturally producing wells are no longer economically viable. A common technique in this area consists of subsea pumping, where electric submersible pumps (ESPs) are used. They are composed of multistage pumps that are known to adapt well to the harsh submarine environments. However, some wells are prone to producing large gas volumes that can drastically affect the overall oil production. This prompted researchers from both industry and academy to investigate centrifugal pumps operating with air-water mixtures, which in fact is not a matter limited to the petroleum industry but also very important for refrigeration loops in nuclear plants.

The experimental studies carried out so far on the subject are mainly concerned with performance evaluation. It is generally found that when pumps operate at part-load liquid flow rates or with high gas concentrations, their performance curves drop significantly. If the gas phase rapidly coalesces and gets stuck inside the pump impellers, the pump head drops remarkably and its operation becomes very unstable, a situation commonly called *surging*. Some authors such as Murakami e Minemura (1974a), Lea e Bearden (1982), Estevam (2002), Barrios (2007) and Gamboa (2008) investigated the gradual performance drop up to the *surging* initiation as a function of the pump rotation speed, gas and liquid flow rates, intake pressure and many other variables. However, few of them, such as Murakami e Minemura (1974a) and Barrios (2007), carried out experimental visualization of the gas phase distribution inside pump impellers to provide a deeper understanding on the phenomenon.

Recent numerical studies on gas-liquid flows in centrifugal pumps are even scarcer and limited to narrow qualitative analysis. For example, Caridad and Kenyery (2004) and Barrios (2007) assumed only the impeller of an ESP stage in a commercial computational fluid dynamics (CFD) package. Using an Eulerian-Eulerian approach, the authors could investigate the distribution of gas at few operating conditions, but only Barrios (2007) managed to compare the flow pattern with actual experimental data, without much exploration of the numerical tool. Before this, Minemura and Murakami (1980) used an Eulerian-Lagrangian "one-way" approach to investigate the motion of independent bubbles in a 5-blade radial impeller. The authors compared trajectories of some bubbles with experimental data, investigated the differences on their paths with the liquid flow streamlines, analyzed the influence of the starting point and the diameter of the bubbles on their resulting trajectory and evaluated force balances on the gas phase. However, their work was very restricted to the assumed pump geometry, and no further advance on testing alternative operating conditions was found since then.

Literature on gas-liquid flows in pumps demands a great amount of descriptive information. The mechanisms behind the dynamics of bubbles, especially their tendency to accumulate in specific parts of the pumps or even the *surging* initiation are still not clear. The role of interfacial forces between gas and liquid should be understood more deeply for that purpose, and numerical tools can be very useful for that. In this context, this work addresses a numerical analysis of the motion of isolated bubbles inside the liquid in a centrifugal pump impeller. CFD is used to perform Eulerian-Lagrangian simulations in order to track the movement of small bubbles inside a pump impeller, for which previous experimental data (Sabino, 2015) is available for comparison. Analyzing the performance of the numerical

model against the experimental visualization data, as well as the sensitiveness of bubbles to different interfacial forces are within the main objectives of this article.

## 2. FLOW MODELING

### 2.1 Equations of motion for a single-phase liquid flow.

Single-phase and isothermal liquid flow inside the pump is governed by continuity and momentum equations. The liquid is assumed as Newtonian and incompressible, with constant density and viscosity. Turbulence is modeled using Reynolds averaging. Adopting the hypotheses above for a rotating frame of reference fixed to the impeller as depicted in Fig. 1, continuity and momentum equations for the liquid phase can be written as:

$$\nabla . \boldsymbol{V}_{xyz} = 0 \tag{1}$$

$$\rho \frac{D\boldsymbol{V}_{xyz}}{Dt} = -\nabla p + \mu_{eff} \nabla^2 . \boldsymbol{V}_{xyz} + \rho_l \boldsymbol{g} - 2\rho_l (\boldsymbol{\Omega} \times \boldsymbol{V}_{xyz}) - \rho_l \boldsymbol{\Omega} \times (\boldsymbol{\Omega} \times \boldsymbol{r}) \,, \tag{2}$$

where $\boldsymbol{V}_{xyz}$ is the velocity vector in the rotating (non-inertial) frame of reference, $\boldsymbol{\Omega}$ is the angular velocity vector, $\boldsymbol{r}$ is the position vector of a liquid particle with respect to the coordinate frame origin, $\rho_l$ is the liquid density, $p$ is the pressure, $\boldsymbol{g}$ is the gravity acceleration and $t$ is time. The effective viscosity, $\mu_{eff}$, is the sum of the liquid dynamic viscosity, $\mu_l$, and the eddy viscosity, $\mu_t$, a term that results from the Reynolds averaging process and the adoption of the Boussinesq hypothesis, and has to be calculated through a turbulence model. The last two terms on the right-hand side of Eq. (2) represent the Coriolis and Centrifugal effects due to the rotating frame of reference. Since a real pump is composed of both static and rotating parts, Eqs. (1) and (2) can be taken generically provided that the Coriolis and Centrifugal effects vanish if a static (inertial) frame of reference is assumed instead.

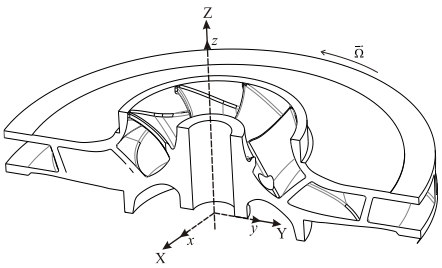


Figure 1. Non-inertial coordinate system for a rotating frame of reference fixed to a centrifugal impeller.

Governing equations must be solved along the whole pump geometry, whose domain is shown schematically in Fig. 2. The pump geometry is based on the two-stage, radial type Imbil® ITAP 65-330/2 centrifugal pump. Here, however, only the first stage is considered. It consists of an intake pipe (static), a radial impeller (rotating), a radial vanned diffuser (static) and a simplified diffuser extension (static) used to locate the pump outlet far from the actual diffuser outlet. The impeller is equipped with 8 blades, whereas the diffuser has 12 vanes. As boundary conditions, a fixed reference pressure is assumed at the intake pipe inlet, while the liquid mass flow rate is specified at the diffuser extension outlet. No-slip conditions are assumed for all walls, but surface roughness is neglected.

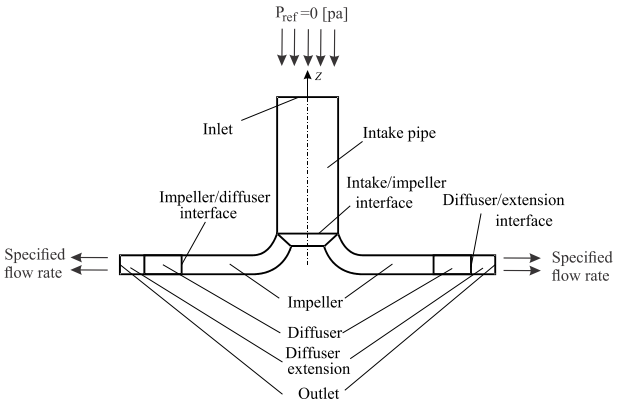

Figure 2. Scheme of the different pump parts that compose the whole numerical domain, with indication of interfaces and boundary conditions (adapted from Sabino, 2015).

**2.2 Equations of motion for bubbles.**

A Lagrangian solution is assumed to model the motion of individual bubbles through the liquid phase inside the pump. This method assumes the bubble as a point-particle, on which Newton's second law is applied to integrate its trajectory from a given initial position up to an arbitrary final integration time or until the particle leaves the solution domain.

A one-way Lagrangian method is adopted, that is, only the liquid phase influences the bubble movement, while the bubble's reaction force on the liquid is neglected, as well as any occasional interaction between different bubbles. As commented by Ansys (2015), this hypothesis is quite satisfactory if the motion of sparsely distributed particles is assumed, as it is indeed the case in this work. Thus, a straightforward solution strategy is adopted in which a steady-state liquid flow field is first calculated through solution of Eqs. (1)-(2), and then the bubble motions are calculated separately. Bubbles are also assumed as small and spherical, and no interphase mass or heat transfer is considered.

Applying Newton's second law on a point-particle of mass $m_p$ yields:

$$m_p \frac{d\boldsymbol{V}_p}{dt} = \sum \boldsymbol{F}_{total} \quad , \tag{3}$$

where $\boldsymbol{V}_p$ is the bubble velocity and $\sum \boldsymbol{F}_{total}$ represent the sum of all forces acting on the bubble that result from its interaction with the surrounding liquid.

The resultant force $\sum \boldsymbol{F}_{total}$ acting on each particle can be roughly divided in two types of forces, one that is meaningful only close to the particle itself and another one that is globally present independently of the particle motion. Next to the particle, the interfacial force, $\boldsymbol{F}_{\text{int}}$, comprises the drag force and another terms that account for the particle acceleration, turbulence of the liquid phase, etc. On the other hand, the field forces that are independent of the particle motion, $\boldsymbol{F}_{field}$, encompasses the gravity force, the pressure gradient force of the liquid phase and the virtual forces that have to be taken into account in a rotating frame of reference. The most relevant forces assumed in literature to compose $\sum \boldsymbol{F}_{total}$ are:

$$\sum \boldsymbol{F}_{total} = \boldsymbol{F}_{\text{int}} + \boldsymbol{F}_{field} = (\boldsymbol{F}_d + \boldsymbol{F}_{\text{vm}} + \boldsymbol{F}_L + \boldsymbol{F}_{WL} + \boldsymbol{F}_{TD} + \boldsymbol{F}_B) + (\boldsymbol{F}_g + \boldsymbol{F}_r + \boldsymbol{F}_p) \tag{4}$$

$\boldsymbol{F}_d$ represents the drag force resulting from any difference on velocities of the bubble and the liquid phase. $\boldsymbol{F}_{\text{vm}}$ is the virtual mass force that arises from the fact that the liquid must be accelerated outside of the bubble trajectory when the latter is moving through the former. $\boldsymbol{F}_L$ is the lift force that a particle experiments in translational motion if the surrounding continuum is a rotational flow (for example a viscous flow). $\boldsymbol{F}_{WL}$ is the wall lubrication force, a term that is only relevant quite close to walls and acts by pushing particles away from it. $\boldsymbol{F}_{TD}$ represents the turbulent dispersion force, a term originated from the turbulence of the liquid phase that tends to disperse high concentrations of particles. $\boldsymbol{F}_B$ is the Basset force, sometimes called as a "delay" force resulting from the time gap between the development of the boundary layer over the particle surface and the actual relative velocity of the particle and the surrounding fluid. $\boldsymbol{F}_g$ is the gravity force, normally associated to buoyancy. $\boldsymbol{F}_r$ is the term that accounts for the fictitious effects due to a rotating frame of reference, that is, the Coriolis and Centrifugal terms. Finally, $\boldsymbol{F}_p$ is the liquid pressure gradient force acting on the bubble. Here, this last force is considered separately from the buoyancy due to the gravity force, being associated to the pressure gradient generated in the pump hydraulic channels due to the centrifugal motion.

Following Minemura and Murakami (1980), the forces that mostly affect the bubble movement are the drag force, the pressure gradient force, the virtual mass force and the force due to the rotating frame of reference. The same hypothesis is assumed in this work so as to neglect many terms in Eq. (4), so that Eq. (3) is given by:

$$m_p \frac{d\boldsymbol{V}_p}{dt} = \boldsymbol{F}_d + \boldsymbol{F}_{\text{vm}} + \boldsymbol{F}_p + \boldsymbol{F}_r, \tag{5}$$

For a spherical bubble of diameter $D$, the drag force acting from the liquid on the bubble is given by:

$$\boldsymbol{F}_d = -\frac{1}{2} C_d \rho_l (\boldsymbol{V}_b - \boldsymbol{V}_l) |\boldsymbol{V}_b - \boldsymbol{V}_l| \frac{\pi D^2}{4}, \tag{6}$$

where $\boldsymbol{V}_b$ is the bubble velocity, $\boldsymbol{V}_l$ is the liquid velocity, $\rho_l$ is the liquid density and $C_d$ is the drag coefficient. This last term is dependent on the particle Reynolds number, which is given by:

$$Re = \frac{\rho_l \, \mathrm{D}(\boldsymbol{V}_b - \boldsymbol{V}_l)}{\mu_l}, \tag{7}$$

where $\mu_l$ is the liquid dynamic viscosity. Within $0 < Re < 1000$, a well-known expression for $C_d$ in terms of $Re$ for spherical particles is given by the Schiller-Naumann correlation (Schiller and Naumann, 1933):

$$C_d = \frac{24}{Re}(1 + 0{,}15Re^{0{,}687}) \ , \tag{8}$$

while $C_d = 0.44$ for higher Reynolds numbers.

The pressure gradient force, $\boldsymbol{F}_p$, is obtained from the solution of the pressure field of the liquid phase. It is proportional to the pressure gradient of the liquid phase, $\nabla p$, and the bubble volume, $\pi D^3 / 6$, and acts on the bubble according to the following expression:

$$\boldsymbol{F}_P = -\frac{\pi D^3}{6} \nabla p \tag{9}$$

Finally, the virtual mass term is proportional to a portion of the mass of liquid displaced by the motion of the bubble and the correspondent acceleration, both in time and space, of the liquid and gas phases. Here, steady-state liquid films are adopted as the continuum through which the particle moves, hence only the advective part of the liquid field acceleration and the Coriolis effect have to be taken into account, resulting in the following expression for the virtual mass force acting on the bubble (Ansys, 2015):

$$\boldsymbol{F}_{\mathrm{vm}} = \frac{C_{\mathrm{vm}}}{2} m_l \left[ -\boldsymbol{V}_l \nabla \boldsymbol{V}_l + 2\Omega \times (\boldsymbol{V}_b - \boldsymbol{V}_l) \right] \ , \tag{10}$$

where $m_l = \rho_l \pi D^3 / 6$ is the mass of the displaced liquid and $C_{\mathrm{vm}}$ is the virtual mass coefficient. For an isolated spherical particle, a value of 0.5 is normally assigned to $C_{\mathrm{vm}}$.

## 3. NUMERICAL PROCEDURE

The solution of the governing equations is carried out through the commercial CFD software ANSYS® CFX® Release 15.0 (Ansys, 2015). Since the centrifugal pump is composed of an assembly of static and rotating parts, a multi-block technique as implemented in the referred CFD program is a good alternative to solve the present problem. In this method, each pump part is assumed as a separate subdomain in which the flow equations are solved in their respective frames of reference. Information is transferred through the subdomains via interface models that may account for the tangential displacement of rotating parts and disarranged meshes between each side of the interface. In the present work, a "Frozen Rotor" model is adopted for the impeller, that is, its rotation is accounted only through the Coriolis and Centrifugal source terms in the momentum equations, while its relative position with respect to the static parts is kept fixed. Steady-state simulations are performed for the liquid phase.

The numerical grid used is shown in Fig. 3. It is composed of body-fitted, hexahedral elements, and was constructed using ANSYS® ICEM CFD™ and ANSYS® TurboGrid™. Advantage from the geometrical periodicity of the pump, was taken, and only 90º in the tangential direction was simulated with help of rotationally periodic boundaries (Ansys, 2015). Special mesh refinement is performed on the pump walls and around the blades. After a mesh sensitivity test, it was verified that a grid with a total number of nodes around 1,200,000 is adequate for the purposes of the present work, where the impeller alone accounts for more than 1,000,000 nodes.

The Finite Volume Method solves Equations (1) and (2) for the liquid. The High-Resolution scheme (Ansys, 2015) is adopted for interpolation of the advection terms. The CFD program assumes co-located grid arrangements for all equations. Regular pressure-velocity coupling methods (such as the SIMPLE-based techniques) are not quite suitable in this case. As discussed by Ansys (2015), an alternative discretization based on the interpolation procedure proposed by Rhie and Chow (1983) is used instead. Turbulence is modeled with the SST $k$-$\omega$ of Menter (1994).

After the solution of the liquid flow field, trajectories of several bubbles are calculated through Eq. (5). The numerical solution is straightforward, using for example the regular first-order Euler integration method (Ansys, 2015).

Initial positions and velocities for the bubbles where gathered from the experimental work of Sabino (2015) for the sake of comparison and validation.

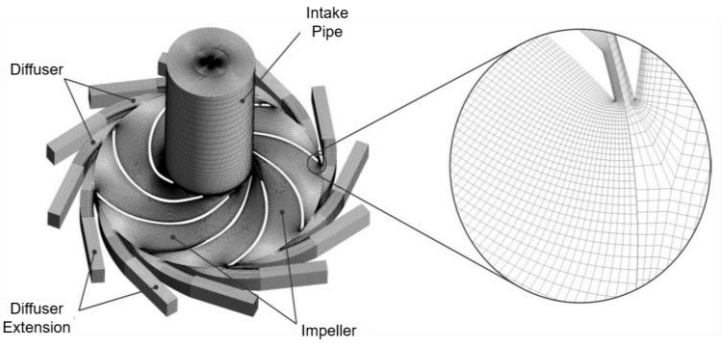


Figure 3: Numerical grid for the first stage of the centrifugal pump (Sabino, 2015).

## 4. RESULTS AND DISCUSSIONS

This section presents the numerical results for the motion of the bubbles inside the centrifugal pump impeller. Results for the bubble trajectories and velocities are compared with experimental data of Sabino (2015). Then, analysis of drag, pressure gradient and virtual mass forces along the bubble trajectories is carried out using data from the numerical simulations.

Table 1 shows some operating conditions used by Sabino (2015) to visualize the motion of individual bubbles inside the pump impeller. The pump speeds adopted by the author range from 100 up to 220 rpm, and the liquid flow rates assumed for each rotating speed range from the best efficiency point (BEP) in each case up to 30% above the BEP flow rate. The same cases are considered here for validation purposes. Before exploring results for the motion of the bubbles, however, the pressure gain obtained for all rotating speeds bellow is compared with data from Sabino (2015).

Table 1: Operating conditions assumed in the simulations (based on Sabino, 2015).

| Pump Speed | Flow rate according to BEP [m 3/h] | | | |
|---|---|---|---|---|
| [rpm] | BEP | 1.1 BEP | 1.2 BEP | 1.3 BEP |
| 100 | 3.18 | 3.50 | 3.82 | – |
| 110 | 3.50 | 3.85 | 4.20 | – |
| 120 | 3.82 | 4.20 | 4.58 | 4.96 |
| 170 | 5.41 | 5.95 | 6.49 | – |
| 220 | 7.00 | 7.70 | 8.40 | – |

### 4.1 Pressure gain through the impeller.

Figure 4 shows the pressure gain through the centrifugal pump impeller with respect to the liquid flow rate for the rotating speeds listed in Tab. 1. Data is computed for single-phase liquid flow. A good agreement between the present numerical results and experimental data from Sabino (2015) is observed. Maximum deviation between all the numerical and experimental values is lower than 6%. The lowest deviations are obtained for flow rates at the best efficiency point, cases where one expects the best performance from the numerical model.

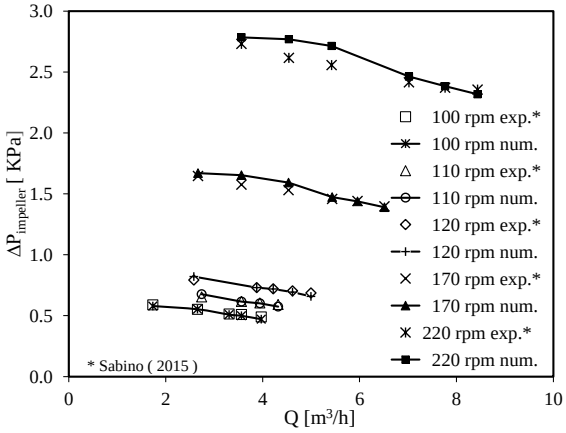

Figure 4. Numerical and experimental results for the pressure gain through the centrifugal impeller for single-phase flow.

**4.2 Bubbles trajectories and velocities inside the impeller.**

Trajectories of bubbles of different diameters experimentally visualized by Sabino (2015) were reproduced in this work for comparison. For a given bubble starting at any point inside the impeller, its initial location and velocity were used as input values for the numerical simulations. Then, the numerically obtained bubble path was compared with the experimental results.

Figure 5 compares numerical and experimental results for the trajectories of bubbles with diameters of 0.51 and 1.16 mm, each obtained for impeller speeds of 100 rpm (at the BEP) and 220 rpm (at 1.2BEP) respectively. The first case consists of a bubble starting from a position close to the impeller suction side, whereas the second one represents the trajectory of a bubble flowing past approximately halfway between the suction and pressure sides of one impeller channel.

For as long as experimental data is available, trajectories obtained from both numerical and experimental results agree quite well. The smallest bubble tends to leave the impeller channel more easily, with a slight path deflection to the pressure side near the exit of the hydraulic channel. The biggest bubble, however, experiments a severe deflection near to the outlet. This effect seems to be influenced by the action of the pressure gradient force, which is directly proportional to the bubble volume. More details on this subject will be discussed later in section 4.3.

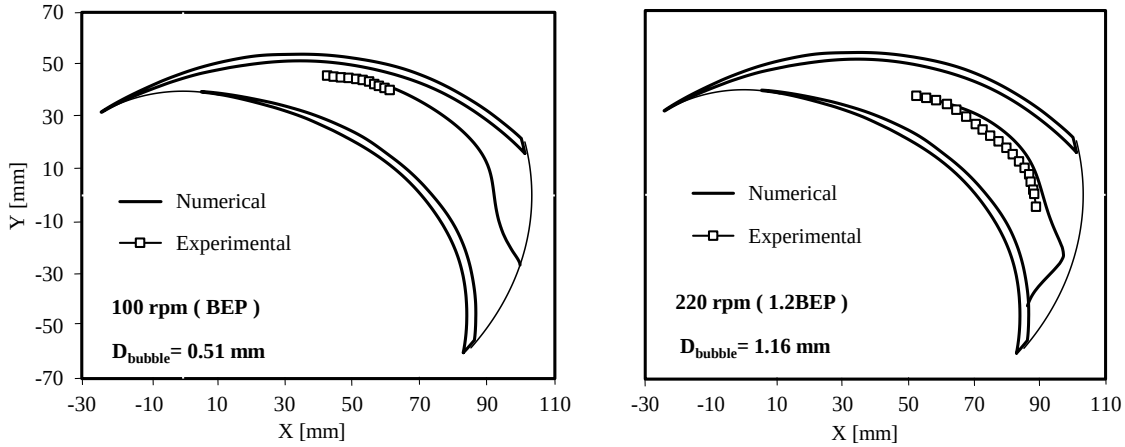


Figure 5. Comparison of numerical and experimental results for trajectories of bubbles with different diameters inside the centrifugal pump impeller.

Figure 6 shows numerical results for the liquid and bubble velocities along each path of the same bubbles analyzed in Fig. 5. In general, one can observe that the liquid velocity is greater than the bubble velocity almost everywhere. An exception is the case for the biggest bubble in regions close to the impeller outlet, where it was observed in Fig. 5 that the bubble is strongly pushed sideways to the blade pressure side. The fact that the liquid velocity is greater than the bubble velocity in most part of its trajectory is also an important effect caused by the pressure gradient of the liquid field acting opposite to the bubble movement. This trend has a great implication on the undesirable *surging* phenomenon, when bubbles are pushed back to the impeller inlet and can rapidly start to coalesce, eventually degrading the pump performance, as extensively discussed by Estevam (2002), Barrios (2007), among others.

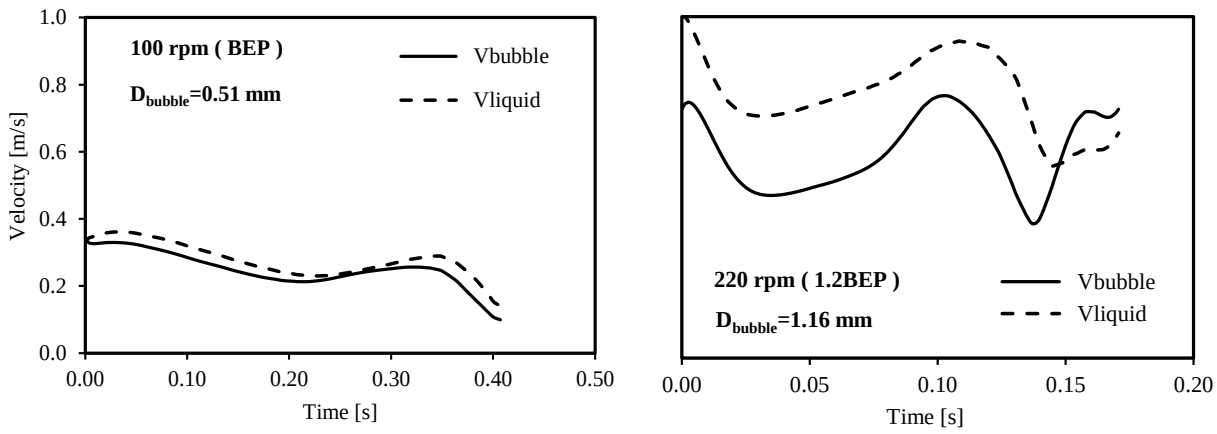

Figure 6. Numerical results for the liquid and bubble velocities along the trajectories of bubbles with different diameters inside the centrifugal pump impeller

**4.3 Forces acting on the bubbles inside the impeller.**

The magnitudes of drag, pressure gradient and virtual mass forces acting on the bubbles along their paths inside the impeller are analyzed in Fig. 7 for two bubble sizes at two different impeller speeds. Values of $F_d$, $F_p$ and $F_{vm}$ are normalized by the external centrifugal force, $F_c = m_p \Omega^2 r_{ext}$, where $\Omega$ is the angular velocity magnitude and $r_{ext}$ is the external radius of the impeller.

For almost the entire path of each bubble, the magnitude of $F_{vm} / F_c$ is the lowest of the three forces considered. In general, the virtual mass force increases reasonably only where great accelerations occur, which happens here at the inlet region and, most notably, at the impeller outlet. Note that the bubble size does not influence this trend in a significant way, as previously suggested by Minemura and Murakami (1980).

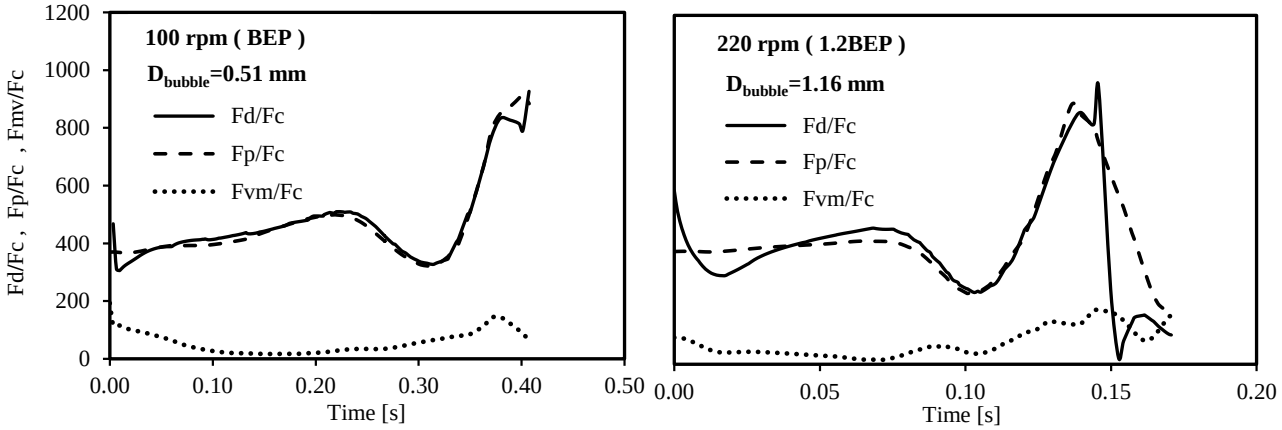


Figure 7. Forces acting on bubbles with diameters of 0.51 mm e 1.16 mm along their trajectories inside the impeller.

On the other hand, the drag and pressure gradient forces are dominant for almost the entire bubble trajectory. In that regard, one can notice that their magnitudes are similar all the way from the inlet to the impeller outlet, indicating that the bubble trajectory is such that $F_d$ constantly tends to a balance with $F_p$. For the smallest bubble, the drag and pressure gradient force magnitudes are almost equivalent from 0.04 s up to 0.14 s, a range where the magnitude of both forces does not vary significantly. A slight increase of $F_p$ is observed from 0.14 s to 0.22 s, followed by a sudden decrease up to 0.32 s. Then, a sharp increase of $F_p$ is observed again up to the end of the bubble trajectory inside the impeller. Close to the end of the bubble trajectory, abrupt variations in $F_d$ are also observed due to quick variations in the bubble velocity. The same general behavior is observed for the biggest bubble, except for a sharp decrease of $F_p$ (followed by a sharp decrease of $F_d$) at the end of the bubble trajectory, where the bubble was severely deflected inside the impeller.

As previously observed in Fig. 6, the liquid velocity is greater than the bubble velocity throughout almost the whole bubble paths, meaning that the drag force acts pushing the bubble towards the impeller outlet most of the time. The pressure gradient force tends to push the bubble in the direction of the impeller inlet, since pressure increases from inlet to outlet in a centrifugal impeller in normal operating conditions. If, at a given point, the pressure gradient increases significantly against the bubble, a deceleration will occur, the liquid relative velocity with respect to the bubble velocity will increase accordingly and the drag force will also increase in response. It should be stressed, however, that these forces do not necessarily act in exact opposite directions, since the drag force acts in the direction of the relative velocity between the bubble and the liquid, while $F_p$ acts in the direction of the pressure gradient of the liquid flow field.

The above results provide a good insight into the complexity in understanding the two-phase flow in centrifugal pumps, but are far from being a comprehensive analysis of the subject. Studying the behavior of gas-liquid mixtures in pumps can be very useful to improve the pumping performance in important industrial areas, but the effect of several variables such as the pump geometry, the flow rates of gas and liquid, the liquid viscosity, among many others, demand supplemental in-depth studies. A good starting point, however, is to investigate the dynamics of isolated bubbles in conditions such as the one carried out in this paper, for which the developed numerical model seems to provide promising results.

## 5. CONCLUSIONS

This work presented a numerical study on the dynamics of gas bubbles flowing through a liquid continuum inside a centrifugal pump impeller. Computational fluid dynamics was used to solve the liquid flow field equations inside the pump, with further tracking of bubble trajectories assuming different diameters and operating conditions.

Comparison of numerical results for the bubble trajectory with previous experimental data showed a good agreement. Analysis of the velocities of the bubbles and the forces acting along their trajectories revealed that drag and the pressure gradient of the liquid field are the dominant forces acting on the bubbles, with a minor influence of the virtual mass force. It could be seen that the drag force, which normally pushes the bubbles outside of the impeller, also acts to balance the pressure gradient force in the opposite direction. High pressure gradients close to the impeller outlet, however, cause lateral deflections in the trajectories of the bubbles, which could lead to a further reverse bubble motion back to the impeller inlet. Deeper study of this behavior for different bubble diameters and off-design operating conditions is the key to understand the *surging* phenomenon, which is an ongoing line of research of this group.

## 6. ACKNOWLEDGEMENTS

The authors acknowledge the financial support from CNPq, ANP and FINEP through the Human Resources Program to oil and gas segment PRH-ANP (PRH 10 - UTFPR) and from TE/CENPES/PETROBRAS.

## 7. REFERENCES

ANSYS, 2015. ANSYS® Academic Research, Release 15.0, Help System, CFX Documentation, ANSYS, Inc.

Asuaje, M., Bakir, F., Kouidri, S., Kenyery F., Rey, R.,2005. Numerical Modelization of the Flow in Centrifugal Pump: Volute Influence in Velocity and Pressure Fields. International Journal of Rotating Machinery, p. 244-255.

Barrios, L. , 2007. Visualization and Modeling of Multiphase Performance inside an Electrical Submersible Pump, PhD dissertation, The University of Tulsa, Tulsa.

Dunaiski, R., 2015, "Simulação Numérica do Escoamento Monofásico em uma Bomba Centrífuga Radial", MS thesis (in Portuguese), Federal Tecnological University of Paraná, Curitiba, Brazil.

Estevam, V. , 2002. Uma análise fenomenológica da operação de bomba centrífuga com escoamento bifásico, PhD thesis (in Portuguese), Faculdade de Engenharia Mecânica, Universidade Estadual de Campinas, Campinas, Brazil.

Gamboa, J., 2008. Prediction of the Transition in Two-Phase Performance of an Electrical Submersible Pump, PhD dissertation, The University of Tulsa, Tulsa.

Gülich, J.F., 2010. Centrifugal Pumps, second ed., Springer-Verlag, Berlin, Germany.

Lea, J.F. and Bearden, J.L., 1982. Effect of Gaseous Fluids on Submersible Pump Performance, Journal of Petroleum Technology, Vol. 34, pp. 2922-2930.

Menter, F.R., 1994. Two-Equation Eddy-Viscosity Turbulence Models for Engineering Applications, AIAA Journal, Vol. 32, pp. 1598-1605.

Murakami, M. and Minemura, K., 1974a. Effects of Entrained Air on the Performance of a Centrifugal Pump (First Report, Performance and Flow Conditions), Bulletin of the JSME, Vol. 17.110, pp. 1047-1055.

Murakami, M. and Minemura, K., 1974b.Effects of Entrained Air on the Performance of a Centrifugal Pump (Second Report, Effects of Number of Blades), Bulletin of the JSME, Vol. 17.112, pp. 1286-1295.

Minemura, K. and Murakami, M., 1980. A Theoretical Study on Air Bubble Motion in a Centrifugal Pump Impeller, Journal of Fluids Engineering, Vol. 102, pp. 446-453.

Rhie, C.M. and Chow, W.L., 1983. Numerical Study of the Turbulent Flow Past an Airfoil with Trailing Edge Separation, AIAA Journal, Vol. 21, pp. 1525-1532.

Sabino, R.H.G., 2015, Análise da Dinâmica de uma Bolha de Gás em uma Bomba Centrífuga , MS dissertation, (in Portuguese), MS thesis (in Portuguese), Federal Tecnological University of Paraná, Curitiba, Brazil.

Schiller, L., Naumann, 1933. A.: VDI Zeits, 77, p. 318.

Segala, W., 2010, "Simulação Numérica do Escoamento Monofásico no Primeiro Estágio de uma Bomba Centrífuga de Duplo Estágio", MS thesis (in Portuguese), Federal Tecnological University of Paraná, Curitiba, Brazil.

Sirino, T., Stel, H., and Morales, R. E. M., 2013, "Numerical Study of the Effect of Viscosity in an Electrical Submersible Pump," Proc. ASME 2013 Fluids Engineering Summer Meeting (FEDSM2013), ASME Digital Collection, pp. V01BT10A026.

Rosa, E. S., 2012, Escoamento Multifásico Isotérmico: Modelo de Multifluidos e de Mistura, Petrobras, Artmed Editora S.A, pp. 197-233.

## 8. RESPONSIBILITY NOTICE

The authors are the only responsible for the printed material included in this paper.